Theoretical Study on the Nonadiabatic Transitions in the Photodissociation Processes of Cl_2

Yukako Asano and Satoshi Yabushita*

Department of Chemistry, Faculty of Science and Technology, Keio University 3-14-1, Hiyoshi, Kohoku-ku, Yokohama 223-8522, Japan

Received: May 30, 2001

Photodissociation of Cl_2 on the shorter wavelength side of the first absorption band has been known to yield a small but significant amount of $Cl(^2P_{1/2})$ from the C $^1\Pi_u$ state, despite its adiabatic correlation to the two $Cl(^2P_{3/2})$ atoms. We calculated some potential energy curves of the ground and excited states of Cl_2 by the spin−orbit configuration interaction method and examined the possibilities of several nonadiabatic transition mechanisms. It was found that the radial Rosen−Zener−Demkov (RZD)-type nonadiabatic transition from the C $^1\Pi_u$ to the third $\Omega = 1_u$ ($^3\Sigma^+_{1u}$ ($\sigma_g \rightarrow \sigma_u^*$)) state is responsible for the production of $Cl(^2P_{1/2})$, and the rotational nonadiabatic transition probability from the C $^1\Pi_u$ to the B $^3\Pi_{0+u}$ state is negligibly small. The wavelength dependence of the product branching ratio $Cl(^2P_{1/2})/Cl(^2P_{3/2})$ and the anisotropy parameter $\beta(Cl(^2P_{1/2}))$, which was calculated from the electronic transition moments to the A $^3\Pi_{1u}$, B $^3\Pi_{0+u}$, and C $^1\Pi_u$ states with the RZD transition mechanism, was in good agreement with their experimental behavior. This RZD model and Young's double slit model could also reproduce the quantum-mechanical interference pattern in the orientation of the total angular momentum $J = {}^1/_2$ of the products $Cl(^2P_{1/2})$.

1. Introduction

Recent advances in both experimental and theoretical studies of molecular photodissociation enable us to investigate quite detailed information on the dissociation dynamics. Special interest has been devoted to molecules with open-shell fragments with nonzero electronic angular momentum, because they would have nearly degenerate asymptotic adiabatic potential energy surfaces and could exhibit significant nonadiabatic interactions. For example, Singer, Freed, and Band[1] stated that if dissociation products have nonzero electronic angular momentum, the Born−Oppenheimer approximation breaks down in the recoupling regions, and neglect of the nonadiabatic interactions brings qualitative disagreement between the theoretical and experimental results.

Therefore, both theoretical and experimental studies of some details such as anisotropy parameters, nonadiabatic transitions, product branching ratios, and orientation and alignment of total angular momentum have been very active subjects, especially for photodissociation of molecules with open-shell fragments with spin−orbit splittings. For example, Hall and Houston[2] discussed photofragment angular momentum polarization in view of some correlations among the vector properties of the photofragments and the parent molecule. Dixon[3] gave a semiclassical description of photofragment angular momentum polarization with bipolar moments and presented detailed equations for the profiles of Doppler-broadened spectral lines. Siebbeles et al.[4] treated quantum-mechanically the dependence of total angular momentum polarization (orientation and alignment) of photofragments and showed the importance of interference effects due to coherent excitation of dissociative states with different helicity quantum numbers. Orr-Ewing and Zare[5] also discussed total angular momentum polarization in terms of orientation and alignment parameters and showed the analytical techniques necessary to obtain them from spectral intensities.

* Corresponding author. Fax: +81-45-566-1697. E-mail: yabusita@chem.keio.ac.jp.

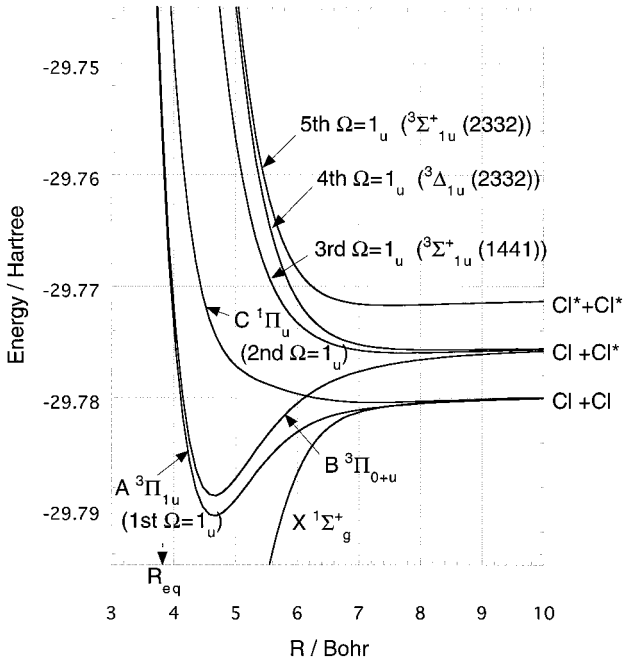

Figure 1. Adiabatic potential energy curves of Cl_2 obtained from the contracted spin−orbit CI calculation. Numbers (*pqrs*) denote the dominant electronic configuration ($\sigma_g^p\pi_u^q\pi_g^{*r}\sigma_u^{*s}$) in the Franck−Condon region.

Molecular chlorine (Cl_2) continues to serve as a benchmark system to study photodissociation dynamics, and many experimental and theoretical studies have been reported. The dissociation products from the first absorption band of Cl_2 are two Cl atoms in the ground-state $Cl(^2P_{3/2})$ or the spin−orbit excited-state $Cl(^2P_{1/2})$ with the spin−orbit splitting of 881 cm^{-1}. In this paper, we denote $Cl(^2P_{3/2})$ and $Cl(^2P_{1/2})$ as Cl and Cl*, respectively. The adiabatic potential energy curves for the ground and relevant excited states are shown in Figure 1. The

10.1021/jp0120561 CCC: $20.00
Published on Web 10/09/2001

first absorption band has a maximum at around 330 nm mainly due to the transition from the X $^1\Sigma^+_g$ to the C $^1\Pi_u$ (second $\Omega = 1_u$) state, which adiabatically correlates to $2 \times$ Cl.[6] Indeed, Colson et al.[7] observed that only Cl products were detected and that the dissociation process was highly adiabatic in the wavelength region between 323.6 and 331.0 nm. Matsumi et al.[8] also observed that the dominant dissociation products were $2 \times$ Cl, but found that a small amount (less than 1%) of Cl* products appeared on the shorter wavelength side of 308 nm with negative anisotropy parameters.

These facts show that the nonadiabatic transition partly occurs from the second $\Omega = 1_u$ (C) state to state(s) dissociating into Cl + Cl* during the bond breaking, as indicated by Matsumi et al.[8] Here, three possibilities for the nonadiabatic transition can be considered: the radial nonadiabatic transition from the second $\Omega = 1_u$ to the third or fourth $\Omega = 1_u$ state ($\Delta\Omega = 0$), the rotational nonadiabatic transition from the second $\Omega = 1_u$ to the B $^3\Pi_{0+u}$ state ($\Delta\Omega = \pm 1$), or combination of these two.

The Landau−Zener (LZ) and Rosen−Zener−Demkov (RZD) models are known as typical models for radial nonadiabatic transitions between adiabatic states with the same symmetry and play an important role in branching phenomena in chemical reactions.[9,10] In the LZ model, the diagonal Hamiltonian matrix elements in diabatic representation, H_{ii} and H_{jj}, cross each other linearly, and the off-diagonal element H_{ij} is constant, giving rise to an avoided crossing. On the other hand, in the RZD model, $\Delta = H_{jj} - H_{ii}$ is constant and H_{ij} depends on the internuclear distance R as $H_{ij} = A \exp(-\alpha R)$. This model has been mainly used for the analyses of near resonant charge-transfer reactions such as $Li^+ + Na \rightarrow Li + Na^+$.[11] Gordon et al.[12] discussed the applicability of the RZD model to the spin−orbit branchings in the photodissociation of oxygen molecules.

Besides, the rotational nonadiabatic transition is another important mechanism, which connects adiabatic states with different symmetries. It is known to play a significant part in predissociation mechanisms, for example, of iodine molecules.[13]

For the previously mentioned nonadiabatic transition in Cl_2, Matsumi et al.[8] suggested that it is the radial nonadiabatic transition from the second $\Omega = 1_u$ state, and Kitsopoulos et al.[14] assumed that it is between the second $\Omega = 1_u$ and B states and follows the LZ behavior. More recently, several experiments on the orientation and alignment in Cl_2 have been reported by Zare et al.[15−18] and Vasyutinskii et al.[19] In particular, Zare et al.[15] observed the interference effects in the orientation of the total angular momentum of the photodissociation products Cl*, and modeled them on the basis of the rotational coupling between the second $\Omega = 1_u$ and B states in order to reproduce the experimental behavior.

An anisotropy parameter β contains important information on photoexcitation, such as directions of the transition moment, but shows little information about the dissociation dynamics after photoexcitation, the shape of potential energy curves far from the Franck−Condon region, and so on. On the other hand, since the interference effects in the orientation of the total angular momentum of the products are quite sensitive to the details of the entire photodissociation processes, their theoretical simulation would provide a wealth of information about the dissociation dynamics. We thus expect that such information may be detailed enough to resolve the previously mentioned controversy on the nonadiabatic mechanisms. Furthermore, since some experimental results are not consistent with one another, it is useful to theoretically analyze details of the experimental results.

Almost two decades ago, Peyerimhoff and Buenker et al.[20] calculated the ground and excited states of Cl_2, and its positive and negative ions, by the multireference single and double excitation configuration interaction method without the spin−orbit interactions. They also calculated the transition moment between the ground and 2 $^3\Pi_u$ excited states by using the first-order perturbed wave functions with the spin−orbit Hamiltonian and analyzed the spin-forbidden transition.[21] More accurate calculation with the spin−orbit Hamiltonian is necessary to analyze the above experimental results in details.

In this study, we calculate the ground and some excited states of Cl_2 by the spin−orbit configuration interaction (SOCI) method and examine the nonadiabatic transition processes that cause branching of the products. It will become clear that the contribution of the radial nonadiabatic transition is dominant, while that of the rotational nonadiabatic transition is negligibly small. This radial nonadiabatic transition is considered to follow the RZD model rather than the LZ model. Furthermore, we analyze the quantum-mechanical interference effects in the orientation of the total angular momentum $J = {}^1/_2$ of Cl* with Young's double slit model to enforce our conclusion for the nonadiabatic mechanism.

2. Computational Methods

We used the RECPs by Christiansen et al.[22] with the valence shell being 3s3p. The associated valence basis functions of 4s4p were used without contraction and augmented by a set of diffuse s and p ($\alpha_s = 0.059\,97$, $\alpha_p = 0.0732$) functions. We added two sets of spherical d-polarization functions ($\alpha_d = 0.7196$ and 0.3671), a set of spherical f-polarization functions ($\alpha_f = 0.5$), and a set of spherical g-polarization functions ($\alpha_g = 0.788$). The basis sets are thus expressed as (5s,5p,2d,1f,1g).

One-electron orbitals for the SOCI calculations must be chosen with a special care to ensure the correct behavior of the potential curves at longer internuclear distances. We have employed the state-averaged SCF molecular orbitals that are optimized for the averaged state of all the configurations derived from (σ_g, π_u, π_g*, σ_u*)[10], namely 10 electrons in the six orbitals. Here, σ_g, π_u, π_g*, and σ_u* are the molecular orbitals derived mostly from 3p atomic orbitals of Cl.

For the SOCI calculations, singlet and triplet configuration state functions (CSF's) were generated with the reference of (σ_g, π_u, π_g*, σ_u*)[10]. All the single and double excitations from these reference CSF's were included in the second-order CI scheme. We carried out the "contracted SOCI" method where the total Hamiltonian including the SO part was diagonalized in the basis of the 16 spin-free CI eigenstates of $3 \times {}^1\Sigma^+_g$, $^1\Pi_{ux}$, $^1\Pi_{gx}$, $^1\Sigma^-_u$, $^1\Delta_g$, $3 \times {}^3\Sigma^+_u$, $^3\Pi_{ux}$, $^3\Pi_{gx}$, $^3\Pi_{uy}$, $^3\Pi_{gy}$, $^3\Sigma^-_g$, and $^3\Delta_u$, all of which correlate with the atomic dissociation limits of Cl(^{2}P) + Cl(^{2}P). The Davidson correction was included in the CI energy. The electronic transition moments and the matrix elements of the L-uncoupling operator were calculated by the first-order SOCI method. All the SOCI calculations were performed with the COLUMBUS program package[23] with an extension of the spin-dependent GUGA.[24,25]

3. Result and Discussion

(1) Adiabatic Potential Energy Curves of Cl_2. Calculated adiabatic potential energy curves are shown in Figure 1. Spectroscopic constants of the X $^1\Sigma^+_g$, A $^3\Pi_{1u}$, and B $^3\Pi_{0+u}$ states are shown in Table 1, and are in reasonable agreement with the experimental values.[26−28] We thus expect that quantitative results can be obtained for the photodissociation processes with these ab initio potential energy curves.

TABLE 1: Calculated and Experimental Spectroscopic Constants for the X $^1\Sigma^+_g$, A $^3\Pi_{1u}$, and B $^3\Pi_{0+u}$ States of Cl_2

		R_e (bohr)	D_e (eV)	ω_e (cm^{-1})	$\omega_e x_e$ (cm^{-1})
X $^1\Sigma^+_g$	this work	3.811	2.335	549.7	2.78
	experiment[26]	3.755	2.475	559.7	2.67
A $^3\Pi_{1u}$	this work	4.662	0.2924	237.5	5.76
	experiment[26,27]	4.597	0.3132	265	5
B $^3\Pi_{0+u}$	this work	4.657	0.3611	240.0	5.26
	experiment[26,28]	4.602	0.3807	259.5	5.3

(2) Absorption Spectra of Cl_2. The first absorption band of Cl_2 has a maximum at around 330 nm mainly due to the spin-allowed vertical excitation from the X $^1\Sigma^+_g$ to the C $^1\Pi_u$ (second $\Omega = 1_u$) state. However, there are some states that are below the C state with nonzero electronic transition moments and can be excited by a photon between 260 and 480 nm. With the spin−orbit interactions, the "good" quantum number for nonrotating linear molecules such as Cl_2 is the *z* (molecular axis) component of the total electronic angular momentum, namely Ω and g−u symmetry. The $^3\Pi_u$ state splits into four sublevels with $\Omega = 2_u$, 1_u, 0^-_u, and 0^+_u, although the magnitude of the splittings is very small especially in the Franck−Condon region. The A $^3\Pi_{1u}$ state has a small configuration mixing with the $^1\Pi_u$ configuration, the B $^3\Pi_{0+u}$ state has a small one with the upper $^1\Sigma^+_u$ configuration, and so on, according to the selection rule for the spin−orbit interactions. The X state also has a small component of $^3\Pi_{0+g}$ besides the dominant $^1\Sigma^+_g$ component. These spin−orbit configuration mixings are the origin of the so-called intensity borrowing of the A and B states. Therefore, the states that are below the C state and can be excited from the X state are the A (via a perpendicular transition, $\Delta\Omega = \pm 1$) and B (via a parallel transition, $\Delta\Omega = 0$) states.

In the numerical calculation of the absorption cross sections, we used the program by Balint-Kurti et al.[29] employing the time-dependent quantum dynamical method.

The calculated absorption spectra to the A, B, and C states are shown in Figure 2. The peak wavelength of the absorption band to the C state is 336.2 nm and in good agreement with the experimental one, which is 331.1 nm by Kitsopoulos et al.[14] The theoretical peak intensity of the first absorption band is weaker than the experimental one of about 0.0027 Å^2. This is mainly because the calculated electronic transition moment, 0.258 D, to the C state at the equilibrium internuclear distance R_e is relatively smaller than the experimentally estimated values, 0.356 D by Coxon[31,32] and 0.371 D by Bayliss.[32] Our value was also a little smaller than other theoretical values, 0.3173 D with the time-dependent Hartree−Fock method and 0.3364 D with the second-order polarization propagator approximation method.[31] At $R = R_e$, the calculated transition moment to the B state was 0.0756 D and that to the A state was 0.0158 D. The corresponding experimental value to the B state is 0.077 D and that to the A state is ∼0.015 D by Coxon.[30] Ishiwata et al.[27] suggested that the ratio of the transition moment to the B state to that to the A state is about 4.8 and in accordance with our theoretical value of 4.79.

The peak intensity of the absorption band to the B state is about 4% of that to the C state, while that to the A state is about 0.3% of that to the C state. These two weak absorption peaks, however, exist far from the peak position of the C state, and their relative intensities become more significant in the longer wavelength region. Therefore, the A and B states are expected to make an important contribution there, despite their weak intensities.

(3) Applicability of the Rosen−Zener−Demkov Model. We first discuss the radial nonadiabatic transition from the second

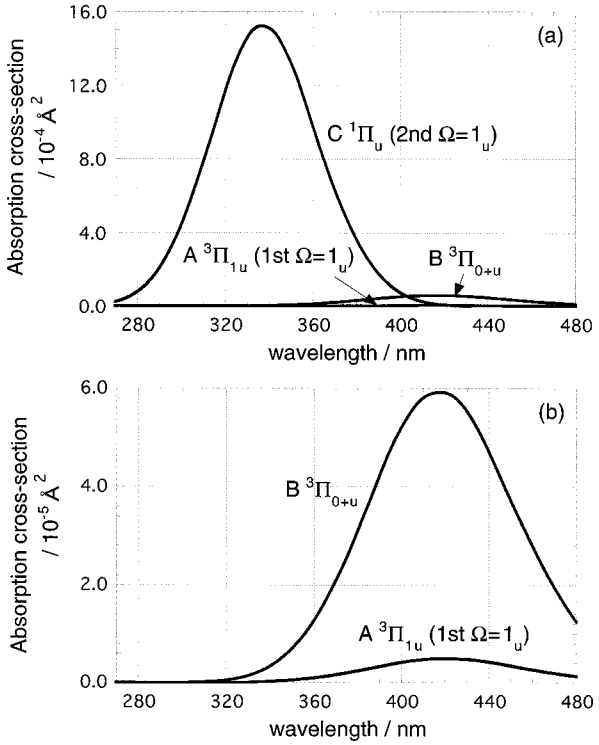

Figure 2. (a) Absorption spectra of Cl_2. (b) Expanded view of (a). The absorption bands to the A $^3\Pi_{1u}$ and B $^3\Pi_{0+u}$ states exist in the edge region of the second $\Omega = 1_u$ (C $^1\Pi_u$) state.

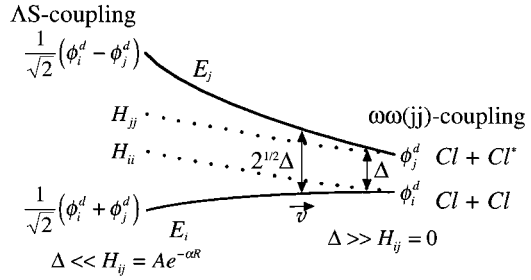

Figure 3. Rosen−Zener−Demkov (RZD) model applied to the nonadiabatic interaction in the dissociation regions of two open-shell atoms with small spin−orbit splittings such as Cl_2. Δ represents $H_{jj} - H_{ii}$ in the diabatic representation. H_{ij} is the exchange interaction between the two atoms caused by the Coulombic interaction and behaves as an exponential function of the internuclear distance *R*.

$\Omega = 1_u$ (C $^1\Pi_u$) to higher state(s) with the same $\Omega = 1_u$ symmetry. Inspecting Figure 1 and the corresponding adiabatic SOCI wave functions does not support the Landau−Zener (LZ)-type behavior for the second $\Omega = 1_u$ state. Instead, we have a theoretical reason for the applicability of the Rosen−Zener−Demkov (RZD) model by considering the behavior of the electronic wave functions.

In the dissociation region, since the Coulombic interaction between the two atoms is very weak, the coupling of the two atomic wave functions is represented better by the *jj*-coupling scheme. Let the two diabatic states be the valence bond type wave functions ϕ_i^d for Cl + Cl and ϕ_j^d for Cl + Cl*, as schematically shown in Figure 3. In this representation, their energy difference $\Delta = H_{jj} - H_{ii}$ corresponds to the spin−orbit splitting between Cl and Cl* and usually shows only a weak dependence on the internuclear distance *R*, especially at longer *R*. Their interaction matrix element H_{ij} corresponds to the exchange interaction caused by the Coulombic interaction between the two atoms and is expected to depend on *R* as

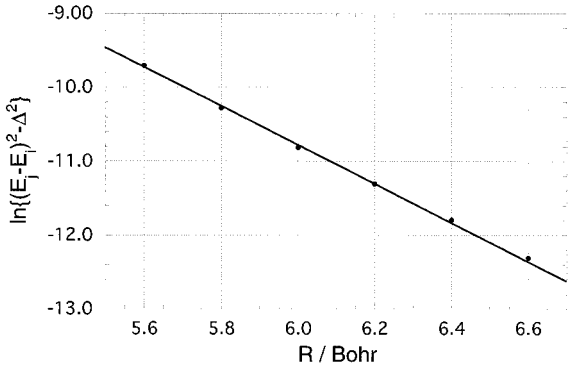

Figure 4. R dependence of the $\ln\{(E_j - E_i)^2 - \Delta^2\}$ value. The parameter fitting is successful and suggests the applicability of the RZD model.

$H_{ij} = A \exp(-\alpha R)$, satisfying the RZD model. As R becomes smaller, namely closer to the Franck−Condon region, the exchange interaction becomes much larger than Δ and the electronic wave functions are appropriately represented by the ΛS-coupling scheme. In particular, the spin−orbit splitting between Cl and Cl* is 881 cm^{-1} and much smaller than that for Br (3685 cm^{-1}) or I (7603 cm^{-1}). Therefore, the ΛS-coupling scheme holds very well in the Franck−Condon region.

If the nonadiabatic interaction follows the RZD model, the radial derivative matrix element between the two adiabatic wave functions Φ_i and Φ_j behaves approximately as

$$g_{ij} = \left\langle \Phi_i \left| \frac{\partial}{\partial R} \right| \Phi_j \right\rangle = \frac{\alpha}{2} \frac{1}{\dfrac{\Delta}{2A \exp(-\alpha R)} + \dfrac{2A \exp(-\alpha R)}{\Delta}} = \frac{\alpha}{4} \frac{1}{\cosh\{\alpha(R - R_{\max})\}} \quad (1)$$

with a peak value of $\alpha/4$ at $R = R_{\max}$, where $A \exp(-\alpha R_{\max}) = \Delta/2$ is satisfied. At $R = R_{\max}$, the exchange interaction and the spin−orbit interaction have an equal magnitude and recoupling of the adiabatic wave functions takes place. The probability of the RZD-type nonadiabatic transition is[9,10]

$$p_{\mathrm{RZD}} = \frac{1}{1 + \exp\left(\dfrac{\pi\Delta}{\hbar v \alpha}\right)} \quad (2)$$

where v is the relative velocity of fragments at $R = R_{\max}$. It follows from eq 2 that as v becomes larger with higher photon energy, p_{RZD} increases.

In the RZD model, the energy difference of the coupled adiabatic energies E_i and E_j would behave as

$$E_j - E_i = \sqrt{4A^2 \exp(-2\alpha R) + \Delta^2} \quad (3)$$

In this study, the three parameters A, α, and Δ were determined by fitting a pair of the coupled SOCI adiabatic energies of the second $\Omega = 1_u$ and third $\Omega = 1_u$ ($^3\Sigma^+{}_{1u}(1441)$) states to eq 3. Here, ($pqrs$) stands for the electronic configuration of $\sigma_g{}^p \pi_u{}^q \pi_g{}^{*r} \sigma_u{}^{*s}$ in terms of the molecular orbitals. These fitted parameters were $A = 6.198\,72$ (hartree), $\alpha = 1.317\,70$ ($bohr^{-1}$), and $\Delta = 4.541\,09 \times 10^{-3}$ (hartree). $R_{\max} = 6.00$ (bohr) was calculated from these parameters. The parameter fitting turned out to be successful, as can be seen from Figure 4, which plots $\ln\{(E_j - E_i)^2 - \Delta^2\}$ vs R.

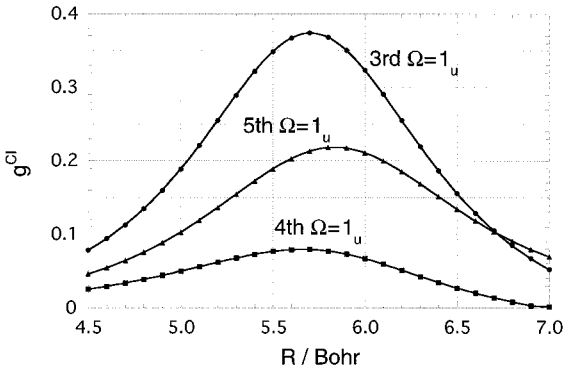

Figure 5. R dependence of the radial derivative coupling matrix elements g^{CI} between the second $\Omega = 1_u$ ($C\ ^1\Pi_u$) and other $\Omega = 1_u$ states. The peak for g^{CI} between the second $\Omega = 1_u$ and third $\Omega = 1_u$ ($^3\Sigma^+{}_{1u}(1441)$) states is larger than the other peaks.

The radial derivative coupling matrix element g_{ij} of eq 1 can also be calculated directly with the CI vectors in the SOCI calculation as follows:[33,34]

$$g_{ij}^{\mathrm{CI}} \approx \sum_k c_{ki}(R) \frac{c_{kj}(R + \Delta R) - c_{kj}(R)}{\Delta R} \quad (4)$$

where c_{ki} is the kth element in the ith CI vector. The step size ΔR in the numerical differentiation was 4.0×10^{-4} bohr in this study. The so-called molecular orbital derivative term was neglected here because its contribution is usually small and to the extent of 10−15%.[34] This approximation is partly justified because the molecular orbitals hardly change at longer R.

Figure 5 shows the R dependence of the matrix elements g_{i2}^{CI} between the ith and second $\Omega = 1_u$ states. Here the nonadiabatic transition from the second $\Omega = 1_u$ to the third $\Omega = 1_u$ state is considered to be much stronger than that to the fourth $\Omega = 1_u$ state. We actually evaluated the latter probability and found it totally negligible.[18] The matrix element g_{52}^{CI} is relatively large, but its transition probability can indeed be neglected because the fifth $\Omega = 1_u$ state correlates to Cl* + Cl*, and Δ in eq 2 in this case corresponds to twice as much as the atomic spin−orbit splitting. It is also in accordance with the fact that the apparent products of Cl* + Cl* have not been observed in any experimental studies. The nonadiabatic transition probability depends not only on the matrix element of the nonadiabatic interaction but also on the adiabatic energy difference.

The RZD parameters, A, α, and Δ can be also obtained by comparing eq 1 with eq 4. We have $A = 14.5150$ (hartree), $\alpha = 1.4959$ ($bohr^{-1}$), $\Delta = 5.7515 \times 10^{-3}$ (hartree), and $R_{\max} = 5.7$ (bohr) in this way. The nonadiabatic transition probability with these parameters is a little smaller than that with the previous parameter set obtained by using only the adiabatic energy differences. Part of this underestimation comes from our approximate evaluation of the matrix element in eq 4. In this study, we thus adopt our previous parameter set and calculate several properties which follow next.

(4) Branching Ratio Cl*/Cl and Anisotropy Parameter β(Cl*) by the RZD Model. From Figure 1, both the A $^3\Pi_{1u}$ and C $^1\Pi_u$ (second $\Omega = 1_u$) states correlate to Cl + Cl. The B $^3\Pi_{0+u}$ state and the third $\Omega = 1_u$ ($^3\Sigma^+{}_{1u}(1441)$) state, to which the RZD-type nonadiabatic transition can occur from the second $\Omega = 1_u$ state, correlate to Cl + Cl*. The branching ratio

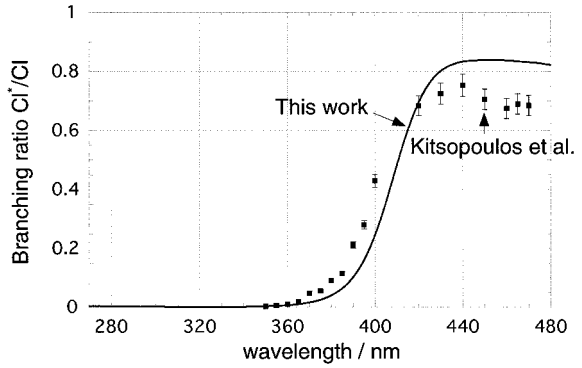

Figure 6. Wavelength dependence of the calculated branching ratio Cl*/Cl compared with the experimental one by Kitsopoulos et al.[14] Note that the values by Kitsopoulos et al.[14] are somewhat different from those by Matsumi et al.[8]

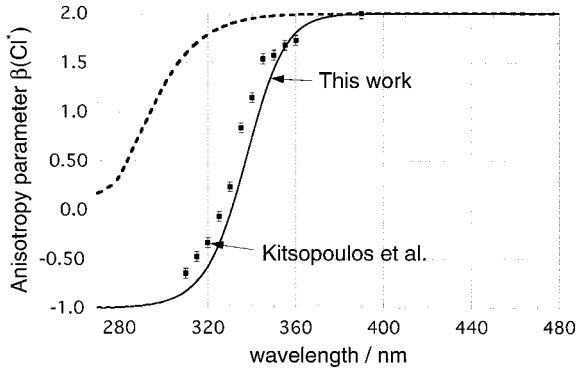

Figure 7. Wavelength dependence of the calculated β(Cl*) compared with the experimental one by Kitsopoulos et al.[14] β(Cl*) calculated with the rotational coupling mechanism at the rotational temperature of 300 K is shown as a dashed line.

Cl*/Cl and the anisotropy parameter β(Cl*) are calculated within axial recoil approximation as follows:

$$\frac{\mathrm{Cl}^*}{\mathrm{Cl}} = \frac{\sigma(\mathrm{B}) + \sigma(\mathrm{C})p_{\mathrm{RZD}}}{\sigma(\mathrm{B}) + \sigma(\mathrm{C})(2 - p_{\mathrm{RZD}}) + 2\sigma(\mathrm{A})} \tag{5}$$

$$\beta(\mathrm{Cl}^*) = \frac{2\sigma(\mathrm{B}) - \sigma(\mathrm{C})p_{\mathrm{RZD}}}{\sigma(\mathrm{B}) + \sigma(\mathrm{C})p_{\mathrm{RZD}}} \tag{6}$$

where p_{RZD} is the probability for the RZD-type nonadiabatic transition from the second $\Omega = 1_u$ to the third $\Omega = 1_u$ state. Here, σ(A), σ(B), and σ(C) are the theoretical photoabsorption cross sections from the X $^1\Sigma^+_g$ to the A, B, and C states, respectively. The wavelength dependence of the calculated Cl*/Cl is shown in Figure 6 and compared with the experimental one by Kitsopoulos et al.[14] It is found that the wavelength dependence of Cl*/Cl can be reproduced, and the orders of the theoretical values of Cl*/Cl at shorter wavelengths are in agreement with the experimental ones despite their small magnitude. The wavelength dependence of the calculated β(Cl*) is shown in Figure 7 and in agreement with the experimental one by Kitsopoulos et al.[14]

We can understand their behavior on the whole as follows. At longer wavelengths, the parallel transition to the B state correlating to Cl + Cl* becomes dominant and β(Cl*) becomes equal to 2. On the other hand, at shorter wavelengths, the perpendicular transition to the C state correlating to Cl + Cl becomes dominant, and β(Cl*) becomes closer to -1 since Cl* is originated by the RZD-type nonadiabatic transition from the second $\Omega = 1_u$ to the third $\Omega = 1_u$ state. The calculated wavelength at which β(Cl*) is equal to zero is around 330 nm and in accordance with the experimental one. As is implied by eq 6, this wavelength critically depends on the balance between the intensity of the absorption bands to the B and C states, and the nonadiabatic transition probability p_{RZD}.

(5) Contribution of the Rotational Nonadiabatic Couplings. We have so far considered only the radial nonadiabatic transitions from the second $\Omega = 1_u$ (C $^1\Pi_u$) to other $\Omega = 1_u$ states. On the other hand, as Figure 1 shows, the second $\Omega = 1_u$ and B $^3\Pi_{0+u}$ states cross each other at $R = 6.17$ bohr. In this section, we discuss whether the rotational nonadiabatic transition between these two states plays an important role.

The form of the rotational Hamiltonian for diatomic molecules in the molecule-fixed coordinate system is as follows:[35]

$$\begin{aligned} H_{\mathrm{rot}} &= \frac{1}{2\mu R^2}[(J^2 - J_z^2) + (L^2 - L_z^2) + (S^2 - S_z^2) \\ &\quad + (L^+S^- + L^-S^+) - (J^+L^- + J^-L^+) - (J^+S^- + J^-S^+)] \\ &= \frac{1}{2\mu R^2}[(J^2 - J_z^2) + (L^2 - L_z^2) + (S^2 - S_z^2)] \\ &\quad + \frac{1}{2\mu R^2}(L^+S^- + L^-S^+) + H_{\mathrm{cor}}^{(L)} + H_{\mathrm{cor}}^{(S)} \end{aligned} \tag{7}$$

where

$$H_{\mathrm{cor}}^{(L)} = -\frac{1}{2\mu R^2}(J^+L^- + J^-L^+) \tag{8}$$

and

$$H_{\mathrm{cor}}^{(S)} = -\frac{1}{2\mu R^2}(J^+S^- + J^-S^+) \tag{9}$$

In this study, the electronic part of the wave function obtained from the SOCI calculation is expanded by the $|\Omega\Lambda S\Sigma\rangle$ basis. When the total wave function consisting of both the electronic and rotational wave functions is considered, it is represented by the $|J\Omega\Lambda S\Sigma\rangle$ basis in Hund's case (a). The first three terms in eq 7 give rise to the rotational energy and the remaining parts correspond to the perturbation terms in the $|J\Omega\Lambda S\Sigma\rangle$ basis. The fourth term is called the spin-electronic operator. The selection rule for the matrix element is $\Delta\Lambda = \pm 1$, $\Delta\Sigma = \mp 1$, $\Delta S = 0$, and $\Delta\Omega = 0$[35] and gives no interaction between the second $\Omega = 1_u$ and B states because of $\Delta\Omega = \pm 1$. The fifth term $H_{\mathrm{cor}}^{(L)}$ and the sixth term $H_{\mathrm{cor}}^{(S)}$ are the so-called Coriolis interaction terms, and are called as the *L*-uncoupling and *S*-uncoupling operators, respectively. The selection rules for these matrix elements are $\Delta\Lambda = \pm 1$, $\Delta\Sigma = 0$, $\Delta S = 0$, and $\Delta\Omega = \pm 1$, and $\Delta\Lambda = 0$, $\Delta\Sigma = \pm 1$, $\Delta S = 0$, and $\Delta\Omega = \pm 1$, respectively,[35] and they depend on the *J* value.

In the Franck−Condon region, according to the selection rules, especially $\Delta S = 0$, neither the *L*-uncoupling nor the *S*-uncoupling operator can connect these two states. They can thus have only indirect second-order interactions as a result of weak spin−orbit configuration mixings.

The situation changes at longer *R*. The B state is a unique $\Omega = 0^+_u$ state that correlates to Cl + Cl* and can be described very well by the $^3\Pi_{0+u}$ configuration even in the dissociation region. On the other hand, both the first and second $\Omega = 1_u$ states correlate to Cl + Cl with significant configuration mixings. These two states in the dissociation region are described by the ΛS-coupling scheme, as follows:[36]

$$|1\text{st } \Omega = 1_u\rangle = \frac{1}{\sqrt{3}}|^3\Pi_{1u}(2431)\rangle + \frac{1}{\sqrt{3}}|^1\Pi_u(2431)\rangle + \frac{1}{\sqrt{3}}|^3\Sigma^+_{1u}(2332)\rangle$$

$$|2\text{nd } \Omega = 1_u\rangle = \frac{\sqrt{2}}{3}|^3\Pi_{1u}(2431)\rangle - \frac{\sqrt{2}}{3}|^1\Pi_u(2431)\rangle + \frac{2}{3}|^3\Sigma^+_{1u}(1441)\rangle + \frac{1}{3}|^3\Delta_{1u}(2332)\rangle$$

According to the selection rules, the $^3\Pi_{0+u}$ ($\Sigma = \pm 1$, $\Lambda = \mp 1$, and $\Omega = 0^+_u$) configuration in the B state can have interactions with the $^3\Pi_{1u}$ ($\Sigma = 0$, $\Lambda = \pm 1$, and $\Omega = 1_u$), $^3\Sigma^+_{1u}$ ($\Sigma = \pm 1$, $\Lambda = 0$, and $\Omega = 1_u$), and $^3\Delta_{1u}$ ($\Sigma = \pm 1$, $\Lambda = \mp 2$, and $\Omega = 1_u$) configurations in the second $\Omega = 1_u$ state. Therefore, the matrix elements between the B state and the following configurations need to be taken into consideration.

L-uncoupling: $^3\Sigma^+_{1u}(1441)$, $^3\Sigma^+_{1u}(2332)$, $^3\Delta_{1u}(2332)$

S-uncoupling: $^3\Pi_{1u}(2431)$

The *R* dependence of the weights of the spin-free components included in the second $\Omega = 1_u$ state shows that the $^1\Pi_u(2431)$ component is dominant at $R = R_e$ (3.8 bohr) but the $^3\Sigma^+_{1u}(1441)$ component cannot be neglected (~30%) at around $R = 6$ bohr. It is necessary to consider the rotational nonadiabatic transition from the second $\Omega = 1_u$ to the B state, because it may occur through the $^3\Sigma^+_{1u}(1441)$ component.

The electronic Hamiltonian H_{el} in the usual CI calculation does not include the molecular rotational Hamiltonian H_{rot} represented by eq 7. H_{rot} acts as perturbation that brings a nonadiabatic transition between the eigenstates of H_{el}. However, the rotational nonadiabatic coupling does not straightforwardly follow the Landau−Zener (LZ) behavior in the usual adiabatic basis. Nakamura[37] defined the dynamical states as the eigenstates of $H_{el} + H_{rot}$. In this dynamical-state representation, $H_{el} + H_{rot}$ is completely diagonal with respect to nuclear rotations and electronic degrees of freedom, and a nonadiabatic transition caused by molecular rotations can be treated as if it were a radial coupling problem.

When a diatomic molecule such as Cl_2 is considered, the dynamical states with the total angular momentum *J* can be expanded in terms of the electronic rotational basis functions $\Psi^J(\Omega)$ defined as

$$\Psi^J(\Omega) = \Phi(\Omega;\mathbf{r}:R)\, Y(J,\Omega;\hat{R}) \tag{10}$$

where $\Phi(\Omega;\mathbf{r}:R)$ is the electronic wave function, $\mathbf{r}$ are the electronic coordinates in the molecule-fixed coordinate system, $Y(J,\Omega;\hat{R})$ is the nuclear rotational wave function, and $\hat{R}$ describes the molecular orientation. The electronic rotational basis functions for the B and second $\Omega = 1_u$ states are written as $\Psi^J(0_u^+)$ and $\Psi^J(\pm 1_u)$, respectively. Here, $\Psi^J(\pm 1_u)$ can be transformed to the following two components with opposite parities.[35]

$$\Psi^J_+(1_u) = \frac{1}{\sqrt{2}}\{\Psi^J(+1_u) + \Psi^J(-1_u)\}$$

$$\Psi^J_-(1_u) = \frac{1}{\sqrt{2}}\{\Psi^J(+1_u) - \Psi^J(-1_u)\} \tag{11}$$

$\Psi^J(0_u^+)$ and $\Psi^J_+(1_u)$ have the same parity and interact with each other, but $\Psi^J_-(1_u)$ has the opposite parity and has no interaction. The matrix elements of the *L*-uncoupling and *S*-uncoupling operators have only to be calculated between $\Psi^J(0_u^+)$ and $\Psi^J_+(1_u)$. Therefore, the eigenvalue problem to be solved for the two states under consideration is

$$\begin{vmatrix} \langle\Phi(0_u^+;\mathbf{r}:R)|H_{el}|\Phi(0_u^+;\mathbf{r}:R)\rangle_{\mathbf{r}} + E_{rot}(0_u^+) - E^J(R) & \langle\Psi^J_+(1_u)|H^{(L)}_{cor} + H^{(S)}_{cor}|\Psi^J(0_u^+)\rangle_{\mathbf{r},\hat{R}} \\ \langle\Psi^J(0_u^+)|H^{(L)}_{cor} + H^{(S)}_{cor}|\Psi^J_+(1_u)\rangle_{\mathbf{r},\hat{R}} & \langle\Phi(1_u;\mathbf{r}:R)|H_{el}|\Phi(1_u;\mathbf{r}:R)\rangle_{\mathbf{r}} + E_{rot}(1_u) - E^J(R) \end{vmatrix} = 0 \tag{12}$$

where the matrix elements of H_{el} are the adiabatic SOCI energies, $E_{rot}(\Omega)$ in the diagonal parts are the rotational energies, and the subscripts $\mathbf{r}$ and $\hat{R}$ describe the integration over all $\mathbf{r}$ and $\hat{R}$. $E_{rot}(\Omega)$ was calculated in the Hund's case (a) basis by

$$E_{rot}(\Omega) = \frac{\hbar^2}{2\mu R^2}\{J(J+1) - 2\Omega^2\} \tag{13}$$

The matrix element of the *L*-uncoupling operator is represented as follows:

$$\langle\Psi^J(0_u^+)|H^{(L)}_{cor}|\Psi^J_+(1_u)\rangle_{\mathbf{r},\hat{R}} = -\frac{1}{2\mu R^2}[J(J+1)]^{1/2}\frac{1}{\sqrt{2}}[\langle\Phi(0_u^+;\mathbf{r}:R)|L^-|\Phi(+1_u;\mathbf{r}:R)\rangle_{\mathbf{r}} + \langle\Phi(0_u^+;\mathbf{r}:R)|L^+|\Phi(-1_u;\mathbf{r}:R)\rangle_{\mathbf{r}}] \tag{14}$$

Furthermore, the brackets in eq 14 lead to

$$\langle\Phi(0_u^+;\mathbf{r}:R)|L^-|\Phi(+1_u;\mathbf{r}:R)\rangle_{\mathbf{r}} = \langle\Phi(0_u^+;\mathbf{r}:R)|L_x - iL_y|\frac{1}{\sqrt{2}}\{\Phi(1_u;\mathbf{r}:R)_x + i\Phi(1_u;\mathbf{r}:R)_y\}\rangle_{\mathbf{r}} = -\sqrt{2}i\langle\Phi(0_u^+;\mathbf{r}:R)|L_y|\Phi(1_u;\mathbf{r}:R)_x\rangle_{\mathbf{r}} \tag{15}$$

and

$$\langle\Phi(0_u^+;\mathbf{r}:R)|L^+|\Phi(-1_u;\mathbf{r}:R)\rangle_{\mathbf{r}} = -\sqrt{2}i\langle\Phi(0_u^+;\mathbf{r}:R)|L_y|\Phi(1_u;\mathbf{r}:R)_x\rangle_{\mathbf{r}} \tag{16}$$

where the subscripts *x* and *y* represent the *x*- and *y*-components in the molecule-fixed coordinate system, respectively. The matrix element of the *L*-uncoupling operator of eq 14 can be rewritten with eqs 15 and 16 as follows:

$$\langle\Psi^J(0_u^+)|H^{(L)}_{cor}|\Psi^J_+(1_u)\rangle_{\mathbf{r},\hat{R}} = \frac{i}{\mu R^2}[J(J+1)]^{1/2}\langle\Phi(0_u^+;\mathbf{r}:R)|L_y|\Phi(1_u;\mathbf{r}:R)_x\rangle_{\mathbf{r}} \tag{17}$$

The *R* dependence of the calculated matrix element of the L_y operator in eq 17 has a maximum at around $R = 6$ bohr due to the *R* dependence of the $^3\Sigma^+_{1u}(1441)$ component in the second $\Omega = 1_u$ state.

On the other hand, as described before, the matrix element of the *S*-uncoupling operator is not zero only when the $^3\Pi_{1u}(2431)$ component in the second $\Omega = 1_u$ state is not zero. Therefore, the matrix element of the *S*-uncoupling operator between the second $\Omega = 1_u$ and B states can be simply estimated from the matrix element between the $^3\Pi_{1u}(2431)$ and the B $^3\Pi_{0+u}$ components, multiplied by $c(^3\Pi_{1u})$, which is the coefficient of the $^3\Pi_{1u}(2431)$ component in the second $\Omega = 1_u$ state.

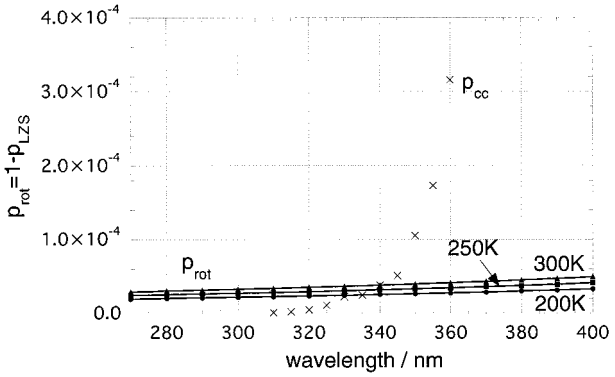

Figure 8. Wavelength dependence of the rotational nonadiabatic transition probability, p_{rot}, calculated by the Landau−Zener-Stueckelberg (LZS) scheme in comparison with p_{cc}, which is the probability that Cl is transferred to Cl* by the nonadiabatic transition from the second $\Omega = 1_u$ to the B $^3\Pi_{0+u}$ state, estimated by Kitsopoulos et al.[14]

$$\langle \Psi^J(0_u^+)|H_{cor}^{(S)}|\Psi_+^J(1_u)\rangle_{\mathbf{r},\hat{\mathbf{R}}} = -\frac{1}{2\mu R^2}\frac{1}{\sqrt{2}}\{[2J(J+1)]^{1/2}c(^3\Pi_{1u}) + [2J(J+1)]^{1/2}c(^3\Pi_{1u})\} = -\frac{1}{\mu R^2}[J(J+1)]^{1/2}c(^3\Pi_{1u}) \quad (18)$$

The eigenvalue including H_{rot} is calculated from eq 12 with the above matrix elements. The radial nonadiabatic transition probability between these two potential energy curves in the dynamical-state representation can be obtained by the semiclassical Landau−Zener−Stueckelberg (LZS)-type expression and actually corresponds to the probability that a fragment still remains on the same adiabatic state after it passes the crossing point in the usual adiabaitc representation. This probability p_{LZS} is calculated from the following expression,[38]

$$p_{LZS} = \exp(-2\delta) \quad (19)$$

where

$$\sigma + i\delta = \frac{1}{v}\int_{R_X}^{R_X^*}\Delta E \, dR \quad (20)$$

$$\Delta E = \sqrt{(E_1 - E_2)^2 + 4H_{12}^2} \quad (21)$$

and v is the velocity at the crossing point, R_X^* is the complex internuclear distance there, R_X is the real part of R_X^*, E_i ($i = 1$ and 2) and H_{12} are the matrix elements in eq 12.

p_{LZS} depends on the total angular momentum J because E_i and H_{12} are functions of J. Assuming that the rotational population follows the Boltzmann distribution, we calculated the p_{LZS} value as a function of the rotational temperature, which was assumed to be 200, 250, or 300 K because we do not have precise information about the experimental one.

The wavelength dependence of the rotational LZS-type nonadiabatic transition probability from the second $\Omega = 1_u$ to the B state, $p_{rot} = 1 - p_{LZS}$, is shown in Figure 8 and is too small to explain the observed results. In fact, if p_{RZD} in eq 6 is replaced by this p_{rot}, β(Cl*) based on the rotational coupling mechanism can be calculated. The wavelength dependence of β(Cl*) thus calculated for 300 K is shown as a dashed line in Figure 7 and deviates from the experimental one very much. We have almost the same rotational transition probability by using the new formula proposed by Nakamura and Zhu.[10] It becomes clear now that the rotational nonadiabatic transition probability is negligibly small, as suggested by Matsumi et al.[8]

(6) Comparison with Other Works. We have so far showed that the RZD-type nonadiabatic transition is the dominant mechanism to yield Cl* from the second $\Omega = 1_u$ ($C\ ^1\Pi_u$), but other groups have considered different nonadiabatic transition processes.

Kitsopoulos et al.[14] estimated the probability that Cl is transferred to Cl* by the nonadiabatic transition from the second $\Omega = 1_u$ to the B $^3\Pi_{0+u}$ state, p_{cc} in Figure 8, as follows:

$$p_{cc} = \frac{A\sigma(B)}{2\sigma(C) + A\sigma(B)} \quad (22)$$

where σ(B) and σ(C) are the partial absorption cross sections from the $X\ ^1\Sigma_g^+$ to the B and C states, respectively, and A is the coefficient of the perpendicular component when the angular distribution of the fragments is represented as $f(\theta) \propto A \sin^2\theta + \cos^2\theta$, where θ is the angle between the fragment recoil direction and the electric polarization vector. They noticed that the behavior of p_{cc} follows the Landau−Zener (LZ)-type relationship,

$$p_{cc} \propto 1 - \exp\left(-\frac{c}{v}\right) \quad (23)$$

where c is a constant and v is the velocity at the crossing point of the two potentials. Although their experimental results approximately followed eq 23 between 310 and 340 nm, they also showed significant deviations at wavelengths longer than 340 nm.

As shown in Figure 8, their p_{cc} value becomes larger as the wavelength is longer, namely, the velocity of the fragment is smaller. On the other hand, the RZD-type nonadiabatic transition probability calculated in this study becomes smaller, as the wavelength is longer. Moreover, the magnitude of their p_{cc} is very different from that of the rotational nonadiabatic transition probability, p_{rot}, calculated in this study, although p_{cc} shows a wavelength dependence similar to that of p_{rot}.

Kitsopoulos et al.[14] further discussed that the nonadiabatic transition may occur at around 3 eV above the zero-point energy of the X state, namely, 0.021 hartree above the dissociation limit of Cl + Cl, and follows the LZ-type behavior according to the velocity dependence of eq 23. Their assumption, however, is not justified because no LZ-type nonadiabatic transition was found in the potential energy curves in Figure 1, and the curve crossing between the second $\Omega = 1_u$ and B states occurs at almost the same energy as the dissociation limit of Cl + Cl.

This difference in the interpretation of the nonadiabatic transition mechanism could originate from the uncertainty of the experimental intensities of the absorption bands. Kitsopoulos et al.[14] had precise information about the branchings only at wavelengths longer than 350 nm, where both the Cl*/Cl and β(Cl*) values were observed. They have obtained the partial absorption cross sections at wavelengths shorter than 350 nm by extrapolating them at the longer wavelengths side. Therefore, their values, in particular at the shorter wavelengths side, might include some errors. In fact, their intensity ratio 4.6×10^3 between the absorption band to the C state and that to the B state amounts to about 5 times of ours 8.9×10^2 at 310 nm.

Zare et al.[15] modeled that Cl* is produced by the rotational nonadiabatic transition from the second $\Omega = 1_u$ to the B state. They estimated that these two potential energy curves cross each other at $R_X = 5.97$ bohr and calculated an effective potential by which the second $\Omega = 1_u$ state could smoothly transfer to

the B state in such a way that the matrix element of the nonadiabatic coupling between them had a maximum at $R = R_X$. They simulated the quantum-mechanical interference effects in the orientation of the total angular momentum $J = {}^1/_2$ of Cl* with this effective potential and obtained fair agreement with experiment. On the other hand, our analysis showed that the rotational nonadiabatic transition probability from the second $\Omega = 1_u$ to the B state is on the order of 10^{-5}, as shown in Figure 8, and is too small to reproduce the wavelength dependence of Cl*/Cl and β(Cl*).

However, Cl* should be produced by some nonadiabatic transitions at around $R = 6$ bohr, because Zare et al.[15] could reproduce the experimental behavior assuming that the matrix element of a nonadiabatic coupling had a maximum at $R_X = 5.97$ bohr. It is interesting that our R_{max} value (6.00 bohr) in the RZD model is very close to their R_X value. In fact, we have seen that the RZD-type nonadiabatic transition from the second $\Omega = 1_u$ to the third $\Omega = 1_u$ state can reproduce the wavelength dependence of Cl*/Cl and β(Cl*). Therefore, we expect that the radial RZD-type nonadiabatic mechanism can also reproduce the interference effects.

(7) The Quantum-Mechanical Interference Effects in the Orientation of the Total Angular Momentum $J = {}^1/_2$ of the Fragment Cl* ($^2P_{1/2}$). Classically, if an electric field oscillates to a direction between parallel and perpendicular to the molecular axis, it induces electronic oscillations in both the parallel and perpendicular directions coherently, that is, with the same phase. According to the potential energy difference between parallel and perpendicular types, the difference in the oscillation frequencies emerges as the molecule dissociates and induces the rotational motion of the electron, namely, the nonstatistical orientation of the angular momentum.[17] Such a preferential orientation is subject to the quantum-mechanical interference effects due to the presence of the two paths, that is, one via the parallel transition ($\Delta\Omega = 0$) and the other via the perpendicular transition ($\Delta\Omega = \pm 1$).

In the wavelength region from 270 to 390 nm, from our previous analysis, such interference effects in the orientation of the total angular momentum $J = {}^1/_2$ of the fragment Cl* are thought to be caused by both Cl* from the B $^3\Pi_{0+u}$ ($\Delta\Omega = 0$) state and Cl* from the third $\Omega = 1_u$ ($^3\Sigma^+_{1u}(1441)$) ($\Delta\Omega = \pm 1$) state produced by the radial RZD-type nonadiabatic transition from the second $\Omega = 1_u$ (C $^1\Pi_u$) state. After an electronic excitation to both the B and C states, the molecule dissociates on the different potentials but finally arrives at the same dissociation products, Cl + Cl*. The potential energy difference produces the phase difference between these two paths and causes the interference effects.

We apply Young's double slit model[39,40] to estimate the interference effects. The total phases for the two dissociation paths given in a semiclassical form are

$$\phi_{2nd\Omega=1_u\rightarrow 3rd\Omega=1_u} = \frac{\pi}{4} + \int_{T_2}^{R_{max}} k_2(R)\,dR + \sigma_0 + \int_{R_{max}}^{\infty} [k_3(R) - k_3(\infty)]\,dR - k_3(\infty)R_{max} \quad (24)$$

$$\phi_{B^3\Pi_{0+u}} = \frac{\pi}{4} + \int_{T_0}^{\infty} [k_0(R) - k_0(\infty)]\,dR - k_0(\infty)T_0 \quad (25)$$

where T_2 is the turning point of the C state for a given photon energy, T_0 is that of the B state for the same energy, and R_{max} is the R value at which the matrix element of the RZD-type nonadiabatic coupling between the second $\Omega = 1_u$ and third $\Omega = 1_u$ states has a maximum. k_n is the wavenumber in relation to the adiabatic energy for the nth state, E_n, as follows:

$$k_n(R) = \frac{1}{\hbar}\sqrt{2\mu\{E - E_n(R)\}} \quad (26)$$

where μ is the reduced mass of Cl_2 and E is the total energy, which is the zero-point energy of the X $^1\Sigma^+_g$ state added to the photon energy. We use $n = 0$ for the B state, $n = 2$ for the second $\Omega = 1_u$ state, and $n = 3$ for the third $\Omega = 1_u$ state. σ_0 in eq 24 is the so-called dynamical phase and represents the additional phase due to the RZD-type nonadiabatic transition.[9]

$$\sigma_0 = \frac{\Delta}{\hbar v \alpha}\{\sqrt{2} - \ln(1 + \sqrt{2})\} \quad (27)$$

where v is the relative velocity at $R = R_{max}$ and Δ and α are the parameters for the RZD model. The phase difference between the two paths is defined as follows:

$$\Delta\phi = \phi_{2nd\Omega=1_u\rightarrow 3rd\Omega=1_u} - \phi_{B^3\Pi_{0+u}} \quad (28)$$

The interference effects between one path via the parallel transition and the other via the perpendicular transition result from the symmetry breaking induced by a mixed transition in which both parallel and perpendicular components are accessed.[40] Quantum-mechanically, the mixed transition is described by a sum of the incoherent and coherent "interference" contributions from parallel and perpendicular transitions.[17] In the case of linearly polarized photolysis light, there only exists the imaginary part of the photofragment orientation parameter, $\mathrm{Im}[\mathbf{a}_1^{(1)}(\parallel,\perp)]$ in the angular momentum distribution. This $\mathrm{Im}[\mathbf{a}_1^{(1)}(\parallel,\perp)]$ parameter is estimated as follows:[15]

$$\mathrm{Im}[\mathbf{a}_1^{(1)}(\parallel,\perp)] \propto |A_\parallel||A_\perp| \sin(\Delta\phi) \quad (29)$$

where $|A_\parallel|$ and $|A_\perp|$ are the coefficients of the transition amplitudes for the parallel and perpendicular transitions, respectively, and $\Delta\phi$ is the phase difference between the parallel and perpendicular paths. For a pure parallel or perpendicular transition, $\mathrm{Im}[\mathbf{a}_1^{(1)}(\parallel,\perp)]$ becomes zero because $|A_\perp|$ or $|A_\parallel|$ in eq 29 is equal to zero.[15] If one parallel and one perpendicular path are considered, eq 29 can be rewritten as[40]

$$\mathrm{Im}[\mathbf{a}_1^{(1)}(\parallel,\perp)] \propto \sqrt{(1+\beta)\left(1 - \frac{\beta}{2}\right)} \sin(\Delta\phi) \quad (30)$$

The calculated $\mathrm{Im}[\mathbf{a}_1^{(1)}(\parallel,\perp)]$ value from eq 30 as a function of an excitation wavelength is compared with the experimental one by Zare et al.[15] in Figure 9. In this calculation, we scaled the calculated potential energies by multiplying a factor of 0.3807/0.3611, because the dissociation energy D_e for the B state was underestimated by this factor.

The wavelength dependence of this interference pattern is in fair agreement with the experimental one, and the isotope effect between ^{35}Cl* and ^{37}Cl* was also reproduced, despite the sensitivity of $\mathrm{Im}[\mathbf{a}_1^{(1)}(\parallel,\perp)]$ to the shape of the potential energy curves. This isotope effect comes from the mass dependence of the phase difference through eq 26.

However, there are some discrepancies between the theoretical and experimental behavior. It may suggest that there still remain errors in the potential energy curves although they were corrected by a scale factor. Moreover, the disagreement may result from the fact that the nonadiabatic transition from the third $\Omega = 1_u$ to the fourth $\Omega = 1_u$ ($^3\Delta_{1u}$) state cannot be neglected. Zare et al.[18] discussed that its transition probability

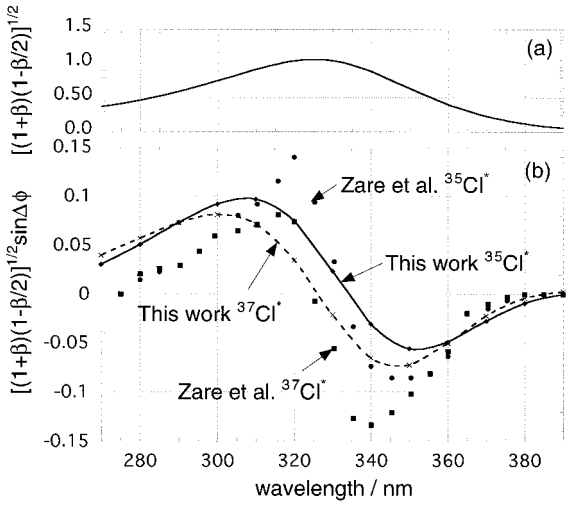

Figure 9. (a) Wavelength dependence of $[(1 + \beta)(1 - \beta/2)]^{1/2}$. (b) Wavelength dependence of the calculated $\mathrm{Im}[\mathbf{a}_1^{(1)}(\parallel,\perp)]$ of $^{35}Cl^*$ and $^{37}Cl^*$ from eq 30 compared with the experimental one by Zare et al.[15] The potential energies were scaled by a factor of 0.3807/0.3611, because the dissociation energy D_e for the B $^3\Pi_{0+u}$ state was underestimated.

was about 20% and might be important. At this moment, we have no conclusive effect by including the fourth $\Omega = 1_u$ state, which has the same dissociation limit, Cl + Cl*, as the third $\Omega = 1_u$ state.

As for the experimental side, Zare[41] suggested that the measurement errors in an anisotropy parameter β might lead to some discrepancies in the wings in the interference pattern because the envelope function $\sqrt{(1+\beta)(1-\beta/2)}$ is very sensitive to the β value. In particular, such sensitivity is more pronounced for the β values for almost pure parallel ($\beta = 2$) and perpendicular ($\beta = -1$) transitions.[42]

As mentioned so far, it is clear that the RZD-type nonadiabatic transition from the second $\Omega = 1_u$ to the third $\Omega = 1_u$ state can explain and reproduce not only the behavior of the branching ratio Cl*/Cl and anisotropy parameter β(Cl*) but also the overall interference pattern. This fact can be a strong evidence that the nonadiabatic transition from the second $\Omega = 1_u$ to state(s) dissociating into Cl + Cl* follows the RZD model.

4. Conclusion

In this work, we have shown that the Rosen−Zener−Demkov (RZD) model can be applied to the noncrossing-type nonadiabatic transitions in the dissociation region of Cl_2.

We calculated the ground and some excited states of Cl_2 by the spin−orbit configuration interaction (SOCI) method and examined the processes of the nonadiabatic transitions that cause the spin−orbit branchings of the products. The radial RZD-type nonadiabatic transition from the second $\Omega = 1_u$ ($C\ ^1\Pi_u$) to the third $\Omega = 1_u$ ($^3\Sigma^+_{1u}(1441)$) state was the dominant mechanism to produce Cl* with the negative anisotropy parameter β(Cl*). The RZD parameters for the transition were $A = 6.198\,72$ (hartree), $\alpha = 1.317\,70$ (bohr^{-1}), and $\Delta = 4.541\,09 \times 10^{-3}$ (hartree). The radial derivative coupling matrix element has a maximum at $R_{max} = 6.00$ (bohr). On the other hand, the rotational nonadiabatic transition probability from the second $\Omega = 1_u$ to the B $^3\Pi_{0+u}$ state was negligibly small.

The branching ratio Cl*/Cl and β(Cl*) were evaluated from the intensities of the absorption bands to the A $^3\Pi_{1u}$, B $^3\Pi_{0+u}$, and C $^1\Pi_u$ states with the RZD transition probability. Their wavelength dependence was well reproduced and originated from the radial RZD-type nonadiabatic transition at shorter wavelengths and from the behavior of the transition moments at longer wavelengths. The RZD model could roughly reproduce the quantum-mechanical interference effects in the orientation of the total angular momentum $J = {}^1/_2$ of the products Cl*.

For further details, it is necessary to calculate the radial derivative coupling matrix elements including the molecular orbital derivative terms with much larger basis set and use a more rigorous quantum-mechanical method to analyze the dissociation dynamics including the fourth $\Omega = 1_u$ state. Such work is now in progress in our laboratory.

Acknowledgment. Some of the present calculations were carried out at the Research Center for Computational Science, Okazaki National Research Institutes. This work was supported in part by a Grants-in-Aid for Scientific Research from the Ministry of Education, Science, Culture, and Sports of Japan and by Research and Development Applying Advanced Computational Science and Technology, Japan Science and Technology Corp. We thank Profs. Dick N. Zare, who suggested this work, Masahiro Kawasaki, Yutaka Matsumi, and T. N. Kitsopoulos and Drs. Andy Alexander and Zee Hwan Kim for useful discussions on their experimental results.

References and Notes

(1) Singer, S. J.; Freed, K. F.; Band, Y. B. *Adv. Chem. Phys.* **1985**, *61*, 1.
(2) Hall, G. E.; Houston, P. L. *Annu. Rev. Phys. Chem.* **1989**, *40*, 375.
(3) Dixon, R. N. *J. Chem. Phys.* **1986**, *85*, 1866.
(4) Siebbeles, L. D. A.; Glass-Maujean, M.; Vasyutinskii, O. S.; Beswick, J. A.; Roncero, O. *J. Chem. Phys.* **1994**, *100*, 3610.
(5) Orr-Ewing, A. J.; Zare, R. N. *Annu. Rev. Phys. Chem.* **1994**, *45*, 315.
(6) Herzberg, G. *Molecular Spectra and Molecular Structure. I Spectra of Diatomic Molecules*; Van Nostrand Reinhold: Princeton, NJ, 1950.
(7) Li, L.; Lipert, R. J.; Lobue, J.; Chupka, W. A.; Colson, S. D. *Chem. Phys. Lett.* **1988**, *151*, 335.
(8) Matsumi, Y.; Tonokura, K.; Kawasaki, M. *J. Chem. Phys.* **1992**, *97*, 1065.
(9) Nikitin, E. E.; Umanskii, S. *Theory of Slow Atomic Collisions*; Springer-Verlag: New York, 1984.
(10) Nakamura, H. *Nonadiabatic Transitions: Beyond Born−Oppenheimer*. In *Dynamics of Molecules and Chemical Reactions*; Wyatt, R. E., Zhang, J. Z. H., Ed.; Marcel Dekker: New York, 1996; p 473.
(11) For example, Dinterman, T. R.; Delos, J. B. *Phys. Rev. A* **1977**, *15*, 463.
(12) Huang, Y.-L.; Gordon, R. J. *J. Chem. Phys.* **1991**, *94*, 2640.
(13) For example, Tellinghuisen, J. *J. Chem. Phys.* **1972**, *57*, 2397. Vigué, J.; Broyer, M.; Lehmann, J.-C. *J. Chem. Phys.* **1975**, *62*, 4941.
(14) Samartzis, P. C.; Bakker, B. L. G.; Rakitzis, T. P.; Parker, D. H.; Kitsopoulos, T. N. *J. Chem. Phys.* **1999**, *110*, 5201.
(15) Kim, Z. H.; Alexander, A. J.; Kandel, S. A.; Rakitzis, T. P.; Zare, R. N. *Faraday Discuss.* **1999**, *113*, 27.
(16) Rakitzis, T. P.; Kandel, S. A.; Alexander, A. J.; Kim, Z. H.; Zare, R. N. *J. Chem. Phys.* **1999**, *110*, 3351.
(17) Alexander, A. J.; Zare, R. N. *Acc. Chem. Res.* **2000**, *33*, 199.
(18) Alexander, A. J.; Kim, Z. H.; Kandel, S. A.; Zare, R. N.; Rakitzis, T. P.; Asano, Y.; Yabushita, S. *J. Chem. Phys.* **2000**, *113*, 9022.
(19) Bracker, A. S.; Wouters, E. R.; Suits, A. G.; Vasyutinskii, O. S. *J. Chem. Phys.* **1999**, *110*, 6749.
(20) Peyerimhoff, S. D.; Buenker, R. J. *Chem. Phys.* **1981**, *57*, 279.
(21) Grein, F.; Peyerimhoff, S. D.; Buenker, R. J. *Can. J. Phys.* **1984**, *62*, 1928.
(22) Pacios, L. F.; Christiansen, P. A. *J. Chem. Phys.* **1985**, *82*, 2664.
(23) Shepard, R.; Shavitt, I.; Pitzer, R. M.; Comeau, D. C.; Pepper, M.; Lischka, H.; Szalay, P. G.; Ahlrichs, R.; Brown, F. B.; Zhao, J.-G. *Int. J. Quantum Chem. Symp.* **1988**, *22*, 149.
(24) Morokuma, K.; Yamashita, K.; Yabushita, S. *Potential Energy Surfaces of Several Elementary Chemical Reactions*. In *Supercomputer Algorithms for Reactivity, Dynamics and Kinetics of Small Molecules*; Laganà, A., Ed.; Kluwer: Dordrecht, The Netherlands, 1989; p 37.
(25) Yabushita, S.; Zhang, Z.; Pitzer, R. M. *J. Phys. Chem. A* **1999**, *103*, 5791.
(26) Huber, K. P.; Herzberg, G. *Constants of Diatomic Molecules*; Van Nostrand Reinhold: New York, 1979.
(27) Ishiwata, T.; Ishiguro, A.; Obi, K. *J. Mol. Spectrosc.* **1991**, *147*, 300.

(28) Coxon, J. A. *J. Mol. Spectrosc.* **1980**, *82*, 264.
(29) Balint-Kurti, G. G.; Mort, S. P.; Marston, C. C. *Comput. Phys. Commun.* **1993**, *74*, 289.
(30) Coxon, J. A. In *Low-lying Electronic States of Diatomic Halogen Molecules*; Barrow, R. F., Long, D. A., Millen, D. J., Eds.; Molecular Spectroscopy Vol. 1; The Chemical Society: London, 1973; p 177.
(31) Ghandour, F.; Jacon, M.; Svendsen, E. N.; Oddershede, J. *J. Chem. Phys.* **1983**, *79*, 2150.
(32) Strempel, J.; Kiefer, W. *J. Chem. Phys.* **1991**, *95*, 2391.
(33) Yabushita, S.; Morokuma, K. *Chem. Phys. Lett.* **1988**, *153*, 517.
(34) Galloy, C.; Lorquet, J. C. *J. Chem. Phys.* **1977**, *67*, 4672.
(35) Lefebvre-Brion, H.; Field, R. W. *Perturbations in the Spectra of Diatomic Molecules*; Academic: New York, 1986.
(36) Nikitin, E. E. *Opt. Spektrosc. (Engl. Transl.)* **1961**, *10*, 227.
(37) Nakamura, H. *J. Phys. Chem.* **1984**, *88*, 4812.
(38) Nakamura, H.; Namiki, M. *Phys. Rev. A* **1981**, *24*, 2963.
(39) Rakitzis, T. P.; Kandel, S. A.; Alexander, A. J.; Kim, Z. H.; Zare, R. N. *Science* **1998**, *281*, 1346.
(40) Rakitzis, T. P.; Zare, R. N. *J. Chem. Phys.* **1999**, *110*, 3341.
(41) Zare, R. N. *Faraday Discuss.* **1999**, *113*, 85.
(42) Zare, R. N. *Faraday Discuss.* **1999**, *113*, 79.